Ceramics International xxx (xxxx) xxx–xxx

Contents lists available at ScienceDirect

Ceramics International

journal homepage: www.elsevier.com/locate/ceramint

Comparative hydrothermal synthesis of hydroxyapatite by using cetyltrimethylammonium bromide and hexamethylenetetramine as additives

Gloria M. Hernández Ortiz, Rodrigo Parra, María A. Fanovich*

Institute of Materials Science and Technology (INTEMA), University of Mar del Plata and National Research Council (CONICET), Av. J. B. Justo 4302, B7608FDQ Mar del Plata, Argentina

ARTICLE INFO

Keywords:
Hydroxyapatite
Hydrothermal synthesis
Nanoparticles

ABSTRACT

Comparative synthesis ways for preparing HA ($Ca_{10}(PO_4)_6(OH)_2$) nanoparticles in presence of hexamethylenetetramine (HMTA) and cetyltrimethylammonium bromide (CTAB) were carried out. The reactions were performed in a Teflon-lined stainless-steel reactor at 120 °C during 12 h. The effects of the additive concentration and the cooling mode (fast and slow) were analyzed. The obtained powders were characterized by X-ray Diffraction (XRD), Raman Spectroscopy, Dynamic Light Scattering (DLS) and Scanning Electron Microscopy (SEM). The two hydrothermal ways carried out for preparing HA nano powders produced a pure crystalline phase of HA. When the fast cooling mode was used, the obtained particles exhibited smaller mean particle sizes. The highest concentrations of used additives (HTMA or CTAB) resulted in opposite effect on the obtained mean particle size of HA particles. These observations were associated to the different behavior of these additives in the HA formation processes.

1. Introduction

Hydroxyapatite (HA, $Ca_{10}(PO_4)_6(OH)_2$), is a calcium phosphate having a similar chemical composition to the inorganic component of bone and teeth. This material is currently used in various forms as a bone substitute due to its properties of biocompatibility, bioactivity and osteoconduction [1,2]. However, nanostructured hydroxyapatite powder has become one of the most useful functional materials in various fields in recent years [3] due to its composition and structure. Owing to their high ion-exchange capacities [4] and strong surface adsorption abilities that result from their surface groups and special chemical constitutions, HA nanomaterials have been widely used in high-capacity drug loading [5–7], protein purification [8], and inorganic and organic pollutants removal from water [9]. Also, as a constituent of composite materials for bone regeneration it has a key role as a bioactive phase [10–13].

The morphology, shape and size of nanoparticles determine the field of application or their suitability for certain needs. Given the importance in controlling the crystalline structure and morphology of HA particles, the implementation of reproducible synthesis techniques becomes crucial. Many methods are known for obtaining HA crystals, namely mechano-chemical [4], sol-gel [4], chemical precipitation [4], hydrothermal [2,14,15], microemulsion [16], ultrasonic irradiation [17] and microwave irradiation [18]. Among them, the hydrothermal method is appropriate for HA nanoparticle synthesis as it yields crystalline HA in a single step under relatively mild reaction conditions [19]. Furthermore, the method allows modifying both size and morphology of the particles by means of the activity of different additives present in the reaction medium. Among the major variables that govern a solvothermal process (nature of reactants, solvent, temperature, pressure, pH and time), the relevance of the cooling rate has not been given serious attention [20]. However, it has been shown that rapid cooling leads to particles of smaller sizes and with higher concentrations of surface defects [21]. Then, as the degree of crystallinity of the material is affected along with the creation of surface defects, rapid cooling is expected to increase the biointegration ability of HA nanoparticles synthesized under hydrothermal reaction conditions.

A further relevant aspect of the solvothermal synthesis of hydroxyapatite, is that nanoparticles with different morphologies, such as spheres, needles, rods, fibers and plates, can be obtained. Such morphologies are achieved using suitable additives that control and lead crystal growth. Among these, cetyltrimethylammonium bromide (CTAB) is a biocompatible cationic surfactant that can be used as additive in many aqueous synthetic methods [22–24]. CTAB ionizes in

* Corresponding author.
E-mail address: mafanovi@fi.mdp.edu.ar (M.A. Fanovich).

https://doi.org/10.1016/j.ceramint.2017.11.120
Received 11 September 2017; Received in revised form 15 November 2017; Accepted 17 November 2017

aqueous solution generating positively charged monomers, which self-assemble into micelles that act as nucleating sites for $(PO_4)^{3-}$ and Ca^{2+} ions on their surfaces to produce HA crystals through a precipitation process [24]. Y. Wang et al. synthesized HA nanoparticles with uniform morphologies and controlled size (mean size about 15 × 150 nm) by low-temperature hydrothermal method in presence of CTAB [23]. Also, Yang et al. prepared HA particles with different morphology as sphere-like colloid, nano-needle to lamellar-like using CTAB/citrate solutions in various concentrations [22]. On the other hand, hexamethylenetetramine (HMTA) is a compound with a cage like structure, which as ligand, presents great versatility allowing different coordination modes. HMTA is highly soluble in water and polar organic solvents, and is a good H-bond acceptor [25]. This cyclic aliphatic amine ($(CH_2)_6N_4$), which has been used for the synthesis of many nanostructured ceramic materials, is seldom used for the synthesis of HA. The article by Andrés-Vergés et al. may have been the first report on the use of HMTA in the synthesis of HA in aqueous medium at 90 °C [26]. The main interest in HMTA resides in its hydroxide anion-generating activity, as it renders ammonia (along with formaldehyde) by means of the hydrolysis reaction that takes place under hydrothermal conditions, gradually raising the pH in the reaction medium [27–29]. Although it has not been clearly demonstrated, HMTA may also have a role as a structure directing agent.

In this context, the aim of this work was to synthesize HA nanoparticles with controlled morphology under hydrothermal conditions in presence of cetyltrimethylammonium bromide and hexamethylenetetramine. The effect of the cooling rate on particle size of the obtained powders was also studied. This work brings new comparative perspectives concerning the influence of CTAB and HTMA on size and shape of HA nanoparticles obtained under hydrothermal conditions.

2. Materials and methods

Calcium hydroxide ($Ca(OH)_2$, Merck), orthophosphoric acid (H_3PO_4, 85%, Merck), hexamethylenetetramine (HMTA, Biopack) and cetyltrimethylammonium bromide (CTAB, Cicarelli) were used as precursors for the synthesis of HA. Fig. 1 shows the followed experimental procedures (with HTMA or CTAB) and Table 1 the selected nomenclature according to the Ca^{2+} to PO_4^{3-} molar ratio, additive used and reactor cooling conditions.

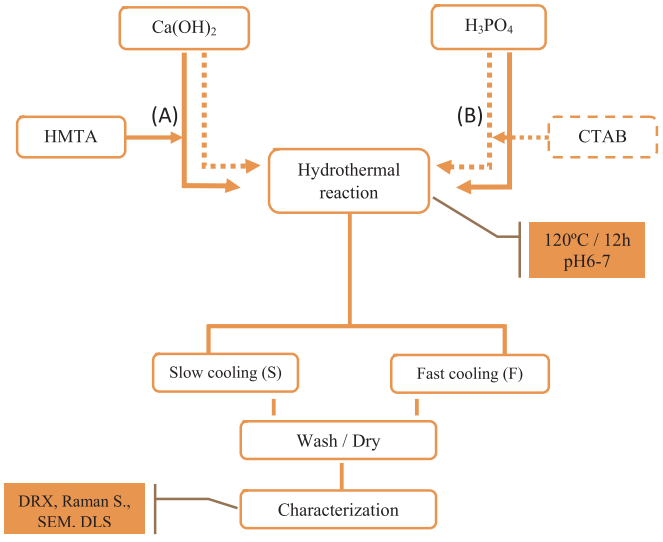

Fig. 1. Flow chart of the experimental procedures for the HA synthesis by using (A) HTMA and (B) CTAB as additives.

Table 1
Hydrothermal HA synthesis conditions from $Ca(OH)_2$ and H_3PO_4 at 120 °C during 12 h.

#	Nomenclature	$Ca(OH)_2$: H_3PO_4 (molar)	Additive	$Ca(OH)_2$:Additive (molar)	Cooling rate
1	F	5:3	–	–	Fast
2	S				Slow
3	HF05		HMTA	1:0.5	Fast
4	HF1			1:1	
5	HS05			1:0.5	Slow
6	HS1			1:1	
7	CF1		CTAB	CMC	Fast
8	CF2			2 x CMC	
9	CS1			CMC	Slow
10	CS2			2 x CMC	

CMC_{CTAB} = 1 mmol/L.

2.1. HA synthesis with HTMA (Procedure A)

Different concentrations of HTMA were used in this set of synthesis. Suspensions of $Ca(OH)_2$ in distilled water were prepared with Ca^{2+} to HMTA molar ratios of 1:0.5 and 1:1. Then, a H_3PO_4 solution (6 mol/L) was slowly added and the reaction mixture was stirred during 5 min. The pH of the resulting mixture was 6. (Fig. 1 (A) solid-line way).

2.2. HA synthesis with CTAB (Procedure B)

A series of synthesis were made with CTAB as additive. A suspension of $Ca(OH)_2$ in distilled water was prepared. Then, CTAB was added to a 6 mol/L H_3PO_4 solution in two concentrations: one in the critical micellar concentration (CMC = 10^{-3} M) and the other at 2 × 10^{-3} mol/L. The phosphoric acid solution (containing CTAB) was slowly poured into the $Ca(OH)_2$ suspension and the resulting mixture was stirred during 5 min. The pH of the final mixture was 6. (Fig. 1 (B) dot-line route).

For both synthesis paths, prepared mixtures were transferred to a 120 mL Teflon-lined stainless-steel reactor, which was put into a furnace for the hydrothermal treatment. For fast cooling, the reactor was withdrawn from the furnace after 12 h at 120 °C and was immersed in an ethylene glycol bath at 0–4 °C. A cooling rate of 2 °C/min was estimated from temperature and time experimental data. In the case of slow cooling, the reactor was kept 12 h at 120 °C and was then cooled to room temperature inside the furnace. In this case, a cooling rate of 0.1 °C/min was estimated from experimental data. Moreover, reaction mixtures without additives were performed following this two cooling procedures as reference syntheses. The final pH measured was 9 for both preparations. In all cases, the obtained products were centrifuged at 5000 rpm, washed with distilled water and dried at 60 °C.

Crystalline HA identification was carried out by X-ray diffraction (XRD) in a PANalytical diffractometer with Cu-Kα radiation (wavelength: λ = 1.54050 Å) at 40 kV and 30 mA. Diffractograms were recorded between 20° and 80° 2θ at a goniometer speed of 1°/min. The mean crystallite size (τ) of the particles was calculated from the XRD line broadening measurement using Scherrer equation:

$$\tau = \frac{0.9\lambda}{\beta cos\theta} \quad (1)$$

Where τ is the crystallite size of the synthesized HA, λ is the wavelength (Cu-Kα), β is the full width at half-maximum of the (002) peak and θ is the corresponding diffraction angle. Raman microspectrometric analyses of HA powders were performed on a multichannel Renishaw In Via Reflex microspectrometer. Excitation was provided by the 785 nm line of an Ar laser. To enhance the signal-to-noise ratio, 30–50 scans were accumulated, each one having a 15 s exposure to laser power ranging between 30 and 300 mW. Raman spectroscopy contributed to the HA phase identification in the samples.

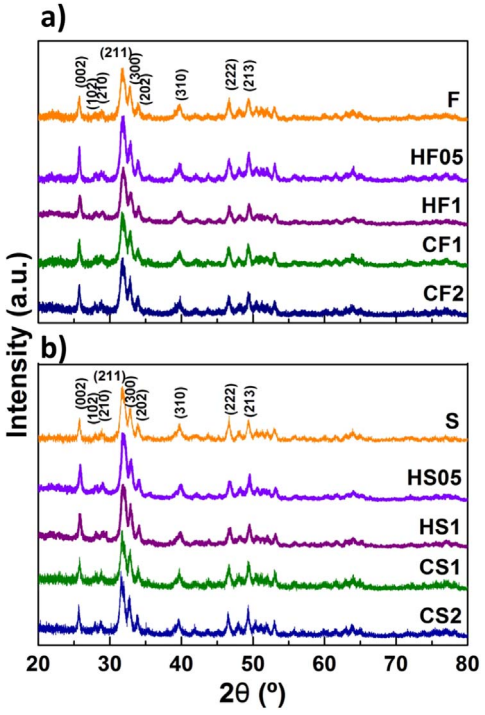

Fig. 2. XRD patterns of the obtained powders: a) fast cooling mode (F series); b) slow cooling mode (S series).

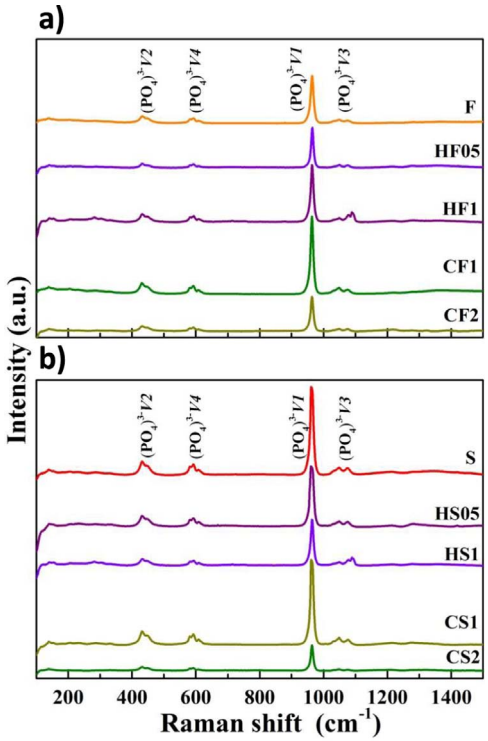

Fig. 3. Raman spectra of the HA powders: a) fast cooling mode (F series); b) slow cooling mode (S series).

Dynamic light scattering (DLS) was performed on powder samples with a Malvern Zetasizer nano S90 with a 532 nm laser. Powders were dispersed in isopropyl alcohol (5 μg in 10 mL) and sonicated for 2 h before each measurement for particle size distribution determination.

Particle morphologies were evaluated by means of scanning electron microscopy (SEM) in a FEI Nanolab 200 FIB/microscope operating at 5 kV. For this purpose, drops of powder dispersions in 2-propanol were deposited on glass slides. After solvent evaporation, the samples were coated with a thin gold layer and examined under different magnifications.

3. Results and discussion

The two hydrothermal routes carried out for preparing HA nano powders produced a pure crystalline phase of HA, as identified by XRD analysis. Fig. 2 shows the X-ray diffraction patterns corresponding to the obtained samples (Table 1). The XRD patterns of samples synthesized in the absence of additives (*S*, F) and in the presence of HMTA (HF05, HF1, HS05, HS1) and CTAB (CF1, CF2, CS1, CS2) revealed the characteristic peaks of HA, in good agreement with the JCPDS 09–0432 file. No significant differences were observed with respect to the signal positions for HA. This may be due to the wide peaks, in accordance with the characteristics of the crystalline nano powders. No preferential growth of the crystals with respect to the use of one additive or another is observed, given that it can be detected by the relative intensities of the signals.

The Raman spectra of the obtained HA powders are shown in Fig. 3. In these spectra, the very strong PO_4 characteristic peak at 961 cm^{-1}, associated with the totally symmetric stretching mode (ν_1: P-O) of the tetrahedral PO_4 group in HA, which is present in the spectra of the samples from all preparations, can be observed. Other bands of lower intensity such as those observed between 450 and 431 cm^{-1}, 610–581 cm^{-1} and 1030–1070 cm^{-1} are due to internal vibrational modes of the phosphate groups in HA: doubly degenerate bending mode (ν_2: O-P-O), triply degenerate bending mode (ν_4: O-P-O) and triply degenerate asymmetric stretching mode (ν_3: P-O) respectively. A very small signal at 1090 cm^{-1} appears only in the samples obtained using high concentration of HTMA in the synthesis (HF1 and HS1 samples). This signal can be assigned to the ν_3 P−O stretching mode of the HPO_4^{2-} group in tricalcium phosphate (TCP) phase [30]. This means that the addition of HTMA into the reaction mixture in high concentration during the (A) synthesis procedure could generate TCP as secondary phase. Anyway, the signal is of very low intensity and the possible presence of crystallized TCP results insignificant, and is below the detection limit of XRD [30]. All these observations are in agreement with the conclusions derived from the XRD patterns confirming the synthesis of crystalline hydroxyapatite.

As was mentioned previously, the surface defects that may be created by rapid cooling of the reaction mixture, are expected to increase the biointegration ability of HA nanoparticles. The features of all obtained XRD spectra are similar. This fact strengthens the idea that cooling modes would only influence the final size of the obtained particles. It is a common practice in hydrothermal synthesis to let the reactor cool slowly, inside the furnace, after a dwell-step at high temperature. In such conditions, the formed particles have enough time to grow and crystallize, so all crystalline particles are obtained. However, if smaller particles are sought, fast cooling is the appropriate way to follow. Fig. 4 shows the effect of cooling rate on morphological features of obtained F and S samples. As can be seen in the images, S sample shows agglomerates of 200–600 nm, while the F sample shows discrete particles with a mean size between 100 and 150 nm with few clusters.

Fig. 5 shows the obtained curves from DLS measurements, to analyze the influence of cooling rate (Fig. 5a), and the effect of type and concentration of additive (Fig. 5b and c). Bimodal size distributions were observed for most samples, in which the high particle-size peak corresponds to clusters of smaller particles. Table 2 summarizes the data extracted from particle size distribution curves.

As shown in Fig. 5a and Table 2, according to DLS measurements, the average size of HA particles was increased more than 80% (106 to195 nm) when the reactor was cooled slowly (*S*) with respect to the measured particle size of the rapidly cooled sample (F). In other words, particle growth is stopped by rapidly cooling the reactor. After this

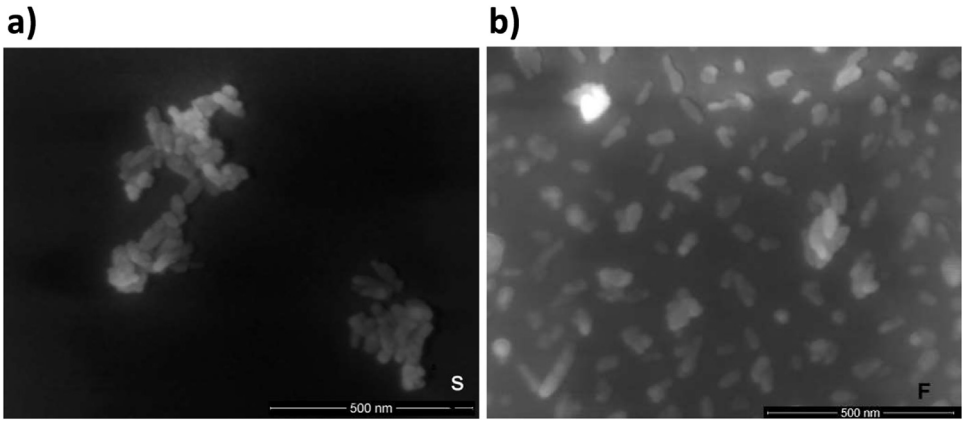

Fig. 4. SEM micrographs of HA particles: a) sample S (slow cooling mode), b) sample F (fast cooling mode).

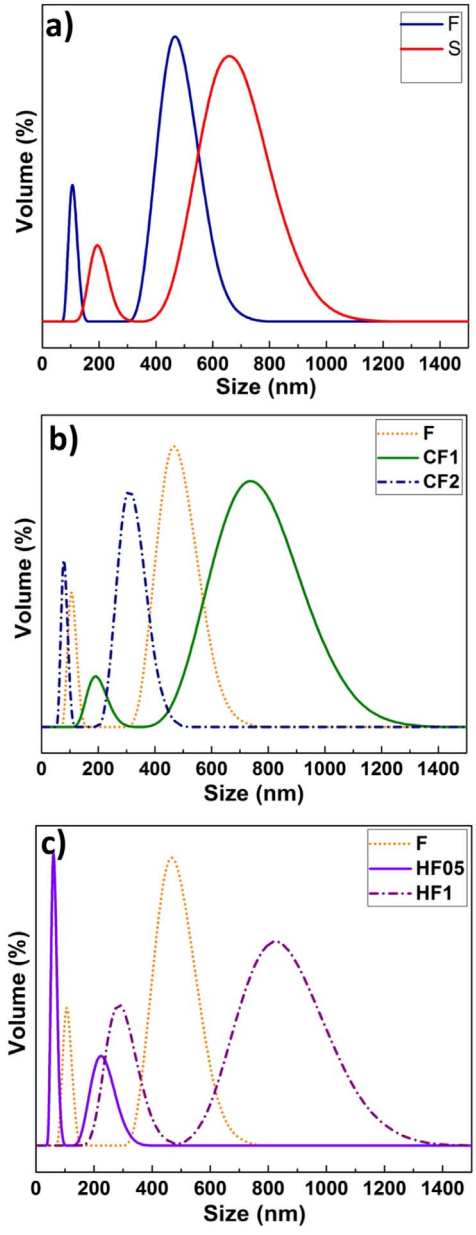

Fig. 5. Particle size distribution curves determined by DLS: a) HA particles obtained without additives, S and F samples, b) HA particles obtained with CTAB and fast cooling mode, c) HA particles obtained with HMTA and fast cooling mode.

Table 2
Analysis of DLS data where 1st and 2nd peaks refer to the low and high particle-size peaks, respectively.

	1st peak			2nd peak		
	FWHM (nm)	Peak (nm)	Volume (%)	FWHM (nm)	Peak (nm)	Volume (%)
S	78	195	20	292	663	80
F	36	106	31	172	473	69
HF05	23	61	74	99	226	26
HS05	76	183	23	283	591	77
HF1	129	289	42	351	831	58
HS1	51	121	11	285	449	89
CF1	83	192	15	82	738	85
CS1	94	194	15	329	872	85
CF2	27	79	39	120	310	61
CS2	71	163	32	333	688	68

FWHM: *full width at half maximum.*

observation, a fast cooling mode was the selected way for the synthesis of HA in the presence of either CTAB or HMTA.

Sample CF1, in which CTAB was used in the critic micellar concentration (1 mmol/L), is composed of high average-size particles within a fairly broad size distribution (Fig. 5b). The minimum average particle size is 192 nm, but majority of particles are forming agglomerates of 740 nm average size. However, when the CTAB concentration was doubled (CF2 in Fig. 5b), smaller particles with an average particle size of 79 nm were obtained. Agglomerates of ~ 300 nm were also detected. This is in agreement with the reports of Ma et al. who showed that the particle size of HA decreased with increasing concentrations of CTAB [31].

On the other hand, the presence of HMTA (HF05) in the reaction medium led to a significant decrease in particle size with respect to sample F, which was obtained without additives. Moreover, the size distribution shows two highly narrow peaks with most of particles (> 70%) within the smaller sizes (~ 60 nm average size) of the distribution and representing the smallest particle size attained in this work (Fig. 5c). When the concentration of HMTA was doubled (HF1), the average particle size increased dramatically, showing an opposed trend to the observed and reported effect of CTAB.

Regarding the role of the additives, that of CTAB is ascribed to the formation of micelles in solution which provide sites for the heterogeneous nucleation of hydroxyapatite. In aqueous solutions, the ammonium moiety in CTAB attracts and concentrates phosphate anions, which trigger HA nucleation and crystallization. When the concentration of CTAB is increased above the CMC, the availability of micelles in solution is also increased, as well as the number of nuclei. Then, the increase in the nuclei concentration leads to a decrease in the average size of final particles.

On the other hand, the role of HMTA on the hydrothermal synthesis of crystalline materials is not fully understood. Although this cyclic tetra-amine has been largely used in the synthesis of zinc oxide nanostructures by chemical bath deposition (CBD) and hydrothermal treatments, conclusions therein have been extrapolated to the synthesis of HA. Two possible mechanisms of action have been proposed for HMTA in hydrothermal syntheses long time ago and the discussion is still under debate. It has been suggested that HMTA provides HO^- ions by means of its slow thermal decomposition into formaldehyde and ammonia. The slow rise in pH would be responsible for the precipitation/crystallization of inorganic materials in hydrothermal reactions [32,33]. In addition, some authors have proposed that HMTA plays a key role as a structure directing agent by complexing ions or adsorbing to specific (non-polar) crystallographic planes of the growing crystal [34]. In order to clarify the effect of HMTA, an aqueous solution of the amine was prepared in this work and treated at 120 °C for 12 h inside the reactor. After the hydrothermal treatment, the pH was observed to rise from 7 to 9. This increase in pH confirms the decomposition of HMTA at high temperature under hydrothermal conditions, but does not rule out its coordination to cations in solution. As was mentioned above, in samples HS1 and HF1 the possible formation of TCP as secondary phase may be due to lower availability of Ca^{2+} when the Ca^{2+}:HMTA ratio was 1:1. Fig. 6 illustrates comparatively the behavior of each additive for the synthesis of HA. It is worth to note that the observed effect of CTAB (sample CF2) on reducing the mean particle size of HA with respect to sample F, was not as significant as the effect of HMTA (sample HF05).

Fig. 7 shows the crystallite size calculated from Scherrer equation of all obtained HA samples. The crystallite sizes were of 36 and 31 nm for S and F samples, respectively. Then, it could be said that the fast cooling rate led to slightly smaller HA nanocrystals. The same effect can be observed between samples HS05/HF05 and HS1/HF1. However, powders obtained by using CTAB showed the largest crystallites. The effect of CTAB could be due to the fact that it generates a higher ordered environment before the precipitation process. So, in fast cooling mode, the crystal is formed from this order, while in the slow cooling mode, dissolution-precipitation processes could take place and consequently crystallite size is reduced.

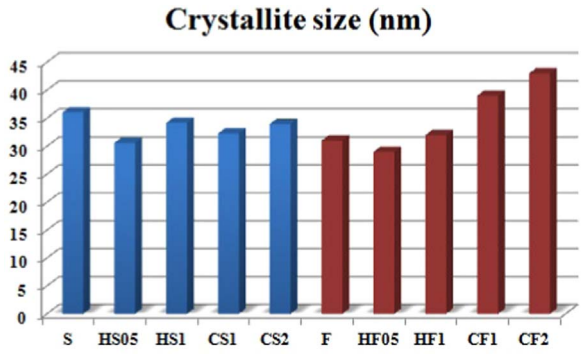

Fig. 7. Crystallite size (nm) of HA samples determined from Scherrer equation.

4. Conclusions

Hydroxyapatite nanoparticles were synthesized by a hydrothermal method with $Ca(OH)_2$ and H_3PO_4 as starting materials. Two types of additives were used: (A) hexamethylenetetramine (HMTA) and (B) cetyltrimethyl ammonium bromide (CTAB). Based on electron microscopy and DLS assays, it was demonstrated that particle size may be tuned by controlling the cooling rate of the reactor. In addition, the use of HMTA or CTBA allows the synthesis of well dispersed HA particles in the nanometer scale. In particular, the use of HMTA in a Ca^{2+}:HMTA 1:0.5 M ratio led to a narrow size distribution of 60 nm average size particles. The highest concentrations of used additives (HTMA or CTAB) showed opposite effects on the final particle size. These observations were associated to the different behavior of these additives in the HA formation process. The effect of CTAB on reducing the mean particle size of HA with respect to obtained sample without additive was not as significant as the effect of HMTA.

Acknowledgements

The authors thank the following institutions for providing financial support: National Research Council (CONICET, Argentina) Project PIP

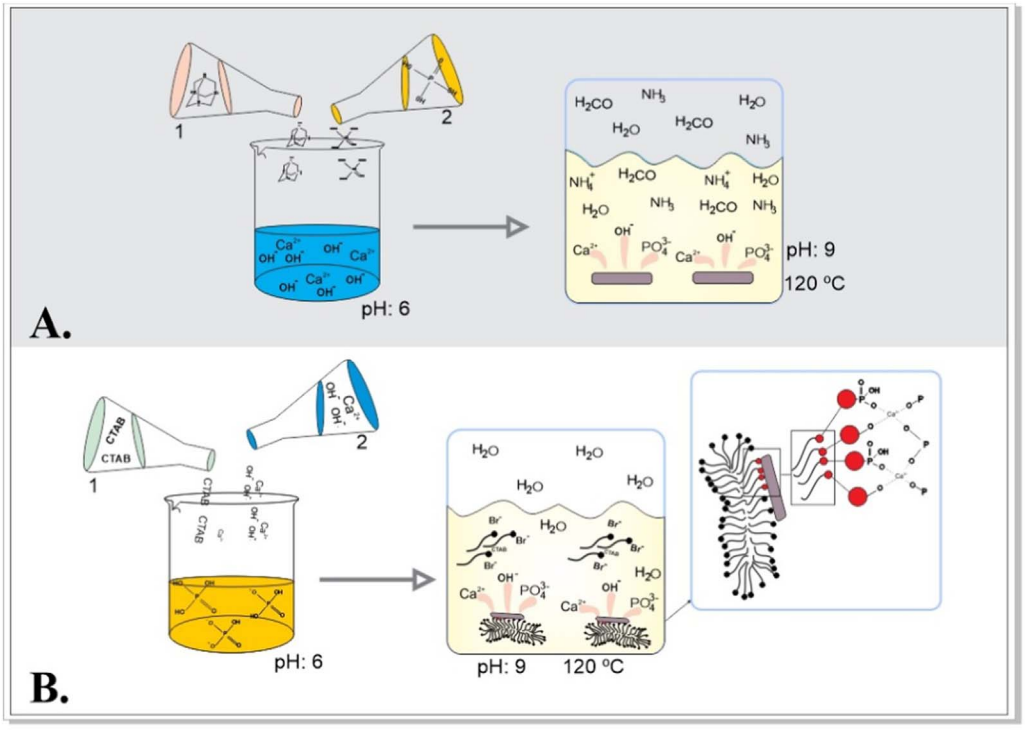

Fig. 6. Schematic representation of the hydrothermal HA synthesis from $Ca(OH)_2$ and H_3PO_4, at 120 °C during 12 h: (A) with HTMA and (B) with CTAB.

1007, University of Mar del Plata (Argentina) Project (15G/454). The collaboration of Martín Lere and R. Savu is acknowledged.

References

[1] K. Loku, S. Yamauchi, H. Fujimori, S. Goto, M. Yoshimura, Hydrothermal preparation of fibrous apatite and apatite sheet, Solid State Ion. 151 (2002) 147–150.
[2] J. Liu, X. Ye, H. Wang, M. Zhu, B. Wang, H. Yan, The influence of pH and temperature on the morphology of hydroxyapatite synthesis by hydrothermal method, Ceram. Int. 29 (2003) 629–633.
[3] C. Li, S. Liu, G. Li, J. Bai, W. Wang, Q. Du, Hydrothermal synthesis of large-sized hydroxyapatite whiskers regulated by glutamic acid in solutions with low supersaturation of precipitation, Adv. Powder Tech. 22 (2011) 537–543.
[4] M. Sadat-Shojai, M. Khorasani, E. Dinpanah-Khoshdargi, A. Jamshidi, Synthesis methods for nanosized hydroxyapatite with diverse structures, Acta Biomater. 9 (2013) 7591–7621.
[5] A.N. Vasiliev, E. Zlotnikov, J.G. Khinast, R.E. Riman, Chemisorption of silane compounds on hydroxyapatites of various morphologies, Scr. Mater. 58 (2008) 1039–1042.
[6] S.J. Segvich, H.C. Smith, D.H. Kohn, The adsorption of preferential binding peptides to apatite-based materials, Biomaterials 30 (2009) 1287–1298.
[7] L.G. Bach, M.R. Islam, Thanh-Sang Vo, S. Kim, K.T. Lim, Poly(allyl methacrylate) functionalized hydroxyapatite nanocrystals via the combination of surface-initiated RAFT polymerization and thiol–ene protocol: a potential anticancer drug nanocarrier, J. Colloid Interface Sci. 394 (2013) 132–140.
[8] J. Sun, L. Wu, Polyether sulfone/hydroxyapatite mixed matrix membranes for protein purification, Appl. Surf. Sci. 308 (2014) 155–160.
[9] Y. Li, H. Zhoua, G. Zhua, C. Shaoa, H. Pana, X. Xu, R. Tanga, High efficient multifunctional Ag_3PO_4 loaded hydroxyapatite nanowires for water treatment, J. Hazard. Mater. 299 (2015) 379–387.
[10] G. Zhang, J. Chen, S. Yang, Q. Yu, Z. Wang, Q. Zhang, Preparation of amino-acid-regulated hydroxyapatite particles by hydrothermal method, Mater. Lett. 65 (2011) 572–574.
[11] S. Pina, J.M. Oliveira, R.L. Reis, Natural-based nanocomposites for bone tissue engineering and regenerative medicine: a review, Adv. Mater. 27 (7) (2015) 1143–1169.
[12] Y. Yang, Q. Wu, M. Wang, J. Long, Z. Mao, X. Chen, Hydrothermal synthesis of hydroxyapatite with different morphologies: influence of supersaturation of the reaction system, Cryst. Growth Des. 14 (2014) 4864–4871.
[13] B. Nasiri-Tabrizi, P. Honarmandi, R. Ebrahimi-Kahrizsangi, P. Honarmandi, Synthesis of nanosize single-crystal hydroxyapatite via mechanochemical method, Mater. Lett. 63 (2009) 543–546.
[14] X. Zhao, Y. Zhu, B. Lu, F. Chen, C. Qi, J. Zhao, J. Wu, Hydrothermal synthesis of hydroxyapatite nanorods using pyridoxal- 5′-phosphate as a phosphorus source, Mater. Res. Bull. 55 (2014) 67–70.
[15] X. Jin, X. Chen, Y. Cheng, L. Wang, B. Hu, J. Tan, Effects of hydrothermal temperature and time on hydrothermal synthesis of colloidal hydroxyapatite nanorods in the presence of sodium citrate, J. Colloid Interface Sci. 450 (2015) 151–158.
[16] X. Ma, Y. Chen, J. Qian, Y. Yuan, C. Liu, Controllable synthesis of spherical hydroxyapatite nanoparticles using inverse microemulsion method, Mater. Chem. Phys. (2016).
[17] M.C. Barbosa, N.R. Messmer, T.R. Brazil, F.R. Marciano, A.O. Lobo, The effect of ultrasonic irradiation on the crystallinity of nano-hydroxyapatite produced via the wet chemical method, Mat. Sci. Eng. C 33 (2013) 2620–2625.
[18] T.T. Demirtaş, G. Kaynak, M. Gümüşderelioğlu, Bone-like hydroxyapatite precipitated from 10 × SBF-like solution by microwave irradiation, Mater. Sci. Eng. C 49 (2015) 713–719.
[19] I.S. Neira, Y.V. Kolen'ko, O.I. Lebedev, G. Van Tendeloo, H.S. Gupta, F. Guitián, M. Yoshimura, An effective morphology control of hydroxyapatite crystals via hydrothermal synthesis, Cryst. Growth Des. 9 (2009) 466–474.
[20] G. Demazeau, Solvothermal processes: definition, key factors governing the involved chemical reactions and new trends, Z. Nat. 65b (2010) 999–1006.
[21] R. Savu, R. Parra, E. Joanni, B. Jančar, S.A. Eliziário, R. de Camargo, P.R. Bueno, J.A. Varela, E. Longo, M.A. Zaghete, The effect of cooling rate during hydrothermal synthesis on ZnO nanorods, J. Cryst. Growth 311 (2009) 4102–4108.
[22] H. Yang, Y. Wang, Morphology control of hydroxyapatite microcrystals: synergistic effects of citrate and CTAB, Mater. Sci. Eng. C 62 (2016) 160–165.
[23] Y. Wang, S. Zhang, K. Wei, N. Zhao, J. Chen, X. wang, Hydrothermal synthesis of hidroxyapatite nanopowders using cationic surfactant as a template, Mater. Lett. 60 (2006) 1484–1487.
[24] M. Khalid, M. Mujahid, S. Amin, R.S. Rawat, A. Nusair, G.R. Deen, effect of surfactant and heat treatment on morphology, surface area and crystallinity in hydroxyapatite nanocrystals, Ceram. Int. 39 (2013) 39–50.
[25] A.M. Kirilov, Hexamethylenetetramine: an old new building block for design of coordination polymers, Coord. Chem. Rev. 255 (2011) 1603–1622.
[26] M. Andrés-Vergés, C. Fernández-González, M. Martínez-Gallego, A new route for the synthesis of calcium-deficient hydroxyapatites with low Ca/P ratio: both spectroscopic and electric characterization, J. Mater. 15 (2000) 11.
[27] J. Shen, B. Jin, Y. Hu, Q. Jiang, An effective route to the synthesis of carbonated apatite crystals with controllable morphologies and growth mechanism, Cryst Eng Comm 17 (2015) 5422–5430.
[28] F. Mohandesa, M. Salavati-Niasari, Z. Fereshtehc, M. Fathi, Novel preparation of hydroxyapatite nanoparticles and nanorods with the aid of complexing agents, Ceram. Int. 40 (2014) 12227–12233.
[29] J. Tao, W. Jiang, H. Pan, X. Xu, R. Tang, Preparation of large-sized hydroxyapatite single crystals using homogeneous releasing controls, J. Cryst. Growth 308 (2007) 151–158.
[30] S. Koutsopoulos, Synthesis and characterization of hydroxyapatite crystals: a review study on the analytical methods, J. Biomed. Mater. Res. 62 (2002) 600–612.
[31] T. Ma, Z. Xia, L. Liao, Effect of reaction systems and surfactant additives on the morphology evolution of hydroxyapatite nanorods obtained via a hydrothermal route, Appl. Surf. Sci. 257 (2011) 4384–4388.
[32] V. Strano, R.G. Urso, M. Scuderi, K.O. Iwu, F. Simone, E. Ciliberto, C. Spinella, S. Mirabella, Double role of HMTA in ZnO nanorods grown by chemical bath deposition, J. Phys. Chem. C 118 (2014) 28189–28195.
[33] K.M. McPeak, T.P. Le, N.G. Britton, Z.S. Nickolov, Y.A. Elabd, J.B. Baxter, Chemical bath deposition of ZnO nanowires at near-neutral pH conditions without hexamethylenetetramine (HMTA): understanding the role of HMTA in ZnO nanowire growth, Langmuir 27 (2011) 3672–3677.
[34] A. Sugunan, H.C. Warad, M. Boman, J. Dutta, Zinc oxide nanowires in chemical bath on seeded substrates: role of hexamine, J. Sol.-Gel Sci. Technol. 39 (2006) 49–56.